ACS APPLIED MATERIALS & INTERFACES

Research Article

www.acsami.org

Templating Quantum Dot to Phase-Transformed Electrospun TiO_2 Nanofibers for Enhanced Photo-Excited Electron Injection

Yakup Aykut,[†] Carl D. Saquing,[‡,§] Behnam Pourdeyhimi,[†] Gregory N. Parsons,[‡] and Saad A. Khan*[,‡]

[†]Fiber and Polymer Science Program, Department of Textile Engineering, Chemistry and Science, North Carolina State University, Raleigh, North Carolina 27695-8301, United States

[‡]Department of Chemical and Biomolecular Engineering, North Carolina State University, Raleigh, North Carolina 27695-7905, United States

Supporting Information

ABSTRACT: We report on the microstructural crystal phase transformation of electrospun TiO_2 nanofibers generated via sol–gel electrospinning technique, and the incorporation of as-synthesized CdSe quantum dots (QDs) to different phases of TiO_2 nanofibers (NFs) via bifunctional surface modification. The effect of different phases of TiO_2 on photo-excited electron injection from CdSe QDs to TiO_2 NFs, as measured by photoluminescence spectroscopy (PL) is also discussed. Nanofiber diameter and crystal structures are dramatically affected by different calcination temperatures due to removal of polymer carrier, conversion of ceramic precursor into ceramic nanofibers, and formation of different TiO_2 phases in the fibers. At a low calcination temperature of 400 °C only anatase TiO_2 nanofiber are obtained; with increasing calcination temperature (up to 500 °C) these anatase crystals became larger. Crystal transformation from the anatase to the rutile phase is observed above 500°C, with most of the crystals transforming into the rutile phase at 800°C. Bi-functional surface modification of calcined TiO_2 nanofibers with 3-mercaptopropionic acid (3-MPA) is used to incorporate as-synthesized CdSe QD nanoparticles on to TiO_2 nanofibers. Evidence of formation of CdSe/TiO_2 composite nanofibers is obtained from elemental analysis using Energy Dispersive X-ray spectroscopy (EDS) and TEM microscopy that reveal templated quantum dots on TiO_2 nanofibers. Photoluminescence emission intensities increase considerably with the addition of QDs to all TiO_2 nanofiber samples, with fibers containing small amount of rutile crystals with anatase crystals showing the most enhanced effect.

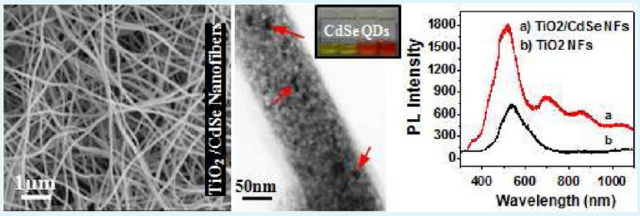

KEYWORDS: *quantum dot, sol–gel electrospinning, nanofibers, photoluminescence*

1. INTRODUCTION

Titanium dioxide (TiO_2) is a wide energy band-gap (anatase, ~3.2 eV and rutile, ~3.0 eV) photoactive semiconductor material that can absorb UV light. Its absorption band can be extended further into the visible region by incorporating narrow band gap dye molecules and semiconductor nanocrystals.[1,2] In addition, TiO_2 also possesses other desirable features, such as strong oxidizing power, nontoxicity, chemical and biological stability, photo induced hydrophilicity, high photoactivity, photodurability, catalytic properties as well as low cost, and good corrosion resistance in aqueous solutions. These attributes make TiO_2 a viable candidate for use in a variety of applications, including dye synthesized solar cells, photocatalysis, photoluminescence, nonlinear optics, humidity and gas sensors, water cleavage, hydrogen and oxygen production from water molecules.[1−5]

The optical and photocatalytic activities of TiO_2 as well as its morphologies and surface chemical and physical properties are affected by its crystal microstructure and intrinsic defects.[1−10] Park et al. reported that the rutile and anatase phases of TiO_2 have essentially the same open circuit photocurrent (V-oc), but the rutile-based cells have about 30% less short-circuit (V-sc) photocurrent than the cells made of the anatase-based TiO_2.[6] Zhang et al. examined the photocatalytic activity of the anatase TiO_2 nanoparticles deposited on the surfaces of rutile particles and observed up to four times enhancement in the activity of these particles.[7] Abazovic et al. found that inherent defects such as oxygen vacancies affected the photoluminescence spectra of anatase and rutile TiO_2 nanoparticles.[10] The characteristic surface functional group (OH) of TiO_2 also plays a significant role in its photocatalytic activity.[8] Moreover, hydrophilicity and hydrophobicity of the surface of TiO_2 materials is affected by crystal morphology.[2] In general, the anatase phase of TiO_2 has been used for catalyst and supports, while rutile TiO_2 because of its high refractive index and dielectric constant, has been used mostly for electronic and optical purposes.[3] In this regard, different crystal phases of TiO_2 have been obtained from the same precursor by varying processing temperature.[3,9]

However, the poor light absorption capability (depending on its intrinsically large energy band gap (~3.2 eV)) limits the use of TiO_2 nanostructures in photovoltaic applications because of inefficient light absorption in the visible region.[2] To overcome

Received: March 25, 2012
Accepted: July 16, 2012
Published: July 16, 2012

 © 2012 American Chemical Society

this limitation, hetero-structured TiO_2 with narrow band gap sensitizer organic dye molecules or inorganic quantum dot semiconductors have been developed and reported on.[11]

Colloidal CdSe quantum dots are small band gap (1.73 eV) spherical, highly emissive inorganic nanoparticles that have unique electroluminescent properties that are dependent on particle size.[12,13] Quantum dot nanoparticles absorb light in the visible region at different wavelengths depending on the particle size.[14] Since they are low band gap semiconductors and their conduction bands are higher than TiO_2, they are favorable for the transfer of excited electrons from their conduction band to TiO_2's conduction band. Likewise, faster electron transfer occurs when particle size is decreased. Their size variation makes them possible to generate multiple exciton from a single photon flux as a result of quantum confinement and impact ionization effects.[15,16] These advantages make QDs as possible replacements for dye molecules. For instance, device performance can be tailored by mixing different sizes of quantum dots as a sensitizer in dye sensitized solar cells.[17]

Despite the strong potential of QDs for use as photonic materials, ways to incorporate them into functional substrates for practical applications have to be sought. Several techniques to incorporate them into ceramic substrates, such as in situ growth of QDs by chemical bath deposition (CBD), deposition of pre-synthesized QDs by direct adsorption (DA), and decoration of pre-synthesized QDs by linker-assisted adsorption (LA) have been reported on by a number of groups.[17] One of the most important properties of QDs is that their size can be controlled, if they are synthesized in reaction media by themselves. Also, for an efficient electron transfer from QDs to TiO_2, better interaction is required at the interface. All of these reasons make the third method, (LA), favorable to produce a QDs/TiO_2 composite nanostructured system for photovoltaic applications.

Since photocatalytic activities mainly take place on the surface of catalyst materials, 1D nanostructured TiO_2 materials are more favorable than any other form of TiO_2, as they combine a high-surface-to-volume ratio with the same amount of materials.[4] Particularly in dye sensitized solar cells, 1D nanofibrous materials are of great interest because more photons can be absorbed by the nanofibers, more dye molecules adhere to the surface, and more electrons are transferred from dye molecules/QDs into the ceramic. This decreases the transit time of the electrons to complete their journeys.[18,19] Furthermore, because of the existence of the direct conduction pathway of the photoelectrons along the fibers, fast and effective electron transfer may be achieved.[20] A variety of 1D fabrication techniques of TiO_2 have thus been examined including hydrothermal method, solvothermal process, direct current magnetron sputtering, atomic layer deposition, sol–gel electrospinning, etc.[4,21−24] Among other methods, sol–gel electrospinning is one of the simplest and more cost effective processes for fabricating TiO_2 nanofibers. To date, electrospun TiO_2 nanofibers from different precursors have been produced by several groups.[4,25−27] Although important in their own rights, what is missing from these studies are (i) systematic preparation of TiO_2 nanofibers with different crystal morphologies, (ii) examination of how these crystal structures affect photoluminescent properties, (iii) incorporation of quantum dots to nanofibers, and (iv) evaluation of concomitant effect of QD-TiO_2 interactions on photoluminescence.

In this study, we show that by systematically varying the calcination temperature of sol-gel produced titanium isopropoxide-polyvinylpyrrolidone nanofibers, TiO_2 nanofibers (NFs) with different morphologies and crystalline phases, from anatase to rutile, can be obtained. These phases strongly influence the optoelectronic properties of the fibers, as observed from photoluminescence spectra. We also synthesized CdSe QDs and incorporate them to the TiO_2 nanofibers via a linker-assisted adsorption (LA) method. Adsorption and linking of CdSe quantum dots onto TiO_2 nanofibers are observed with FTIR and EDS spectra, while direct visualization of the CdSe quantum dots templating on the surface of TiO_2 nanofibers were evaluated via transmission electron microscopy (TEM). The incorporation of QDs enhances the photoluminescence emission intensities and can be maximized with judicious choice of the TiO_2 nanofiber crystal morphology.

2. EXPERIMENTAL SECTION

Chemicals. For electrospinning TiO_2 nanofibers, stock solution of polyvinylpyrrolidone (PVP) as carrier polymer with a molecular weight of 1300 kDa, Ti (IV) isopropoxide as ceramic precursor, and ethanol and acetic acid as solvents were used. For cadmium selenide (CdSe) QD nanoparticles synthesis, cadmium oxide, oleic acid, selenium, trioctylphosphine, and octadecane were used. As a linker, bifunctional chemical reagent 3-mercaptroprionic acid (3-MPA) was used, and for QD suspension preparation and washing of the final composite structure tetrahydrofuran (THF) was used. All materials were purchased from Sigma-Aldrich, USA, and used as received without any purification.

Sol–Gel Electrospinning of TiO_2 Nanofibers. The specifics of the sol–gel electrospinning process, based on the work of Ramakrishna et al.,[25] are briefly described here whereas a schematic representation of the procedure is shown in Supporting Information Figure 1. First, 0.5 g of PVP was dissolved in 6.25 g ethanol. Then 0.5 g of Ti (IV) isopropoxide was added into a polymer solution and magnetically stirred for 2 h. Subsequently, 2.25 g acetic acid was added into an alkoxide precursor solution for ageing. The stock solution was then stirred at 50°C for 30 minutes and left at room temperature for 6 h to develop into an appropriate gel solution. After the desired viscosity was obtained, ∼1 mL of the Ti(IV) isopropoxide/PVP/ethanol/acetic acid ceramic precursor stock solution was loaded into a syringe fitted with a stainless steel needle (0.508 mm i.d.) and attached to a power supply (Gamma High Voltage Research, D-ES 30PN/M692). A flow rate of 0.5 mL/h was used. The collecting distance between the tip and the needle was 15 cm. The grounded collector plate was covered with aluminum foil. A voltage of 12 kV was applied.

The electrospinning stock solution parameters were measured at ambient condition (25 °C). The viscosity was 0.11 Pa.s (TA Instruments AR-2000 rheometer using a 40 mm diameter, 2° cone and plate geometry), the electrical conductivity was 18.76 μS, and the surface tension was 26.8 ±0.5 dyn.cm^{-1} (Fisher Surface Tensiometer, Model 20). To remove organic components from the ceramic system and convert the ceramic precursor into fully crystalline ceramic nanofibers a Model 58114 Lindberg one zone furnace with a quartz tube inner diameter of 45 mm was used. For the calcination process, the temperature was increased from 400 to 500, 650, and 800 °C in air, separately for each sample group, with a heating rate of 5°C/min. This temperature was maintained for 3 h to remove the polymer carrier and to obtain the desired crystal phases of the TiO_2 nanofibers.

One-Step CdSe Quantum Dot (QD) Synthesis. CdSe quantum dot nanoparticles with a variety of sizes were synthesized using non-coordinating solvents, as has been reported by Nordell et al. and Yu et al.[13,28,29] On the basis of this procedure, 30 mg of Se and 5 ml octadecane were measured and placed in a 10 mL round bottom flask which was then clamped over a stirrer on a hot plate. Trioctylphosphine (0.4 mL) was extracted via a syringe from the Sure-Seal bottle. It was then placed in the same 10 mL flask. The prepared mixture was stirred with a magnetic stir bar until dissolution

of Se. The solution was stored at room temperature as a precursor for CdSe quantum dot nanoparticle synthesis. CdO (13 mg) was added into a 25 mL round bottom flask and clamped in a heating mantle. In the same flask, 0.6 mL of oleic acid and 10 mL of octadecane were added. The temperature of the prepared mixture was controlled using a temperature controller with a thermocouple, and the mixture was heated while stirring with a magnetic stir bar. When the temperature reached 225°C, 1 mL of the previously prepared Se solution was measured with a syringe and transferred into the cadmium solution and was allowed to form and grow CdSe QD nanoparticles. After all of the chemicals were added into the reaction mixture, different sizes of as-synthesized QDs were extracted from the reaction media at 10 second intervals.

Oleic acid-terminated CdSe QD nanoparticles were separated from octadecane solvent using a procedure that involved the use of ethanol.[29] Octadecane CdSe suspension was transferred into a micro centrifuge tube up to its midpoint (Figure 1Aa) and fully filled up with

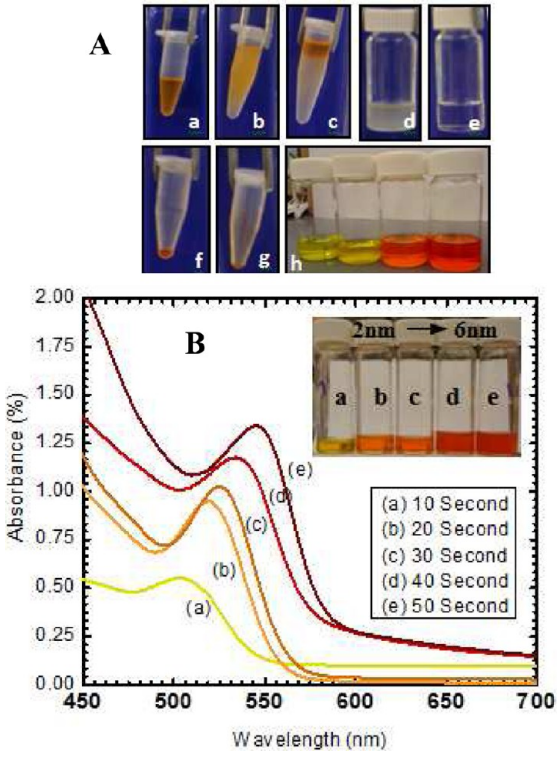

Figure 1. (A) Isolation steps of CdSe quantum dots from octadecane: (a) CdSe in octadecane and oleic acid; (b) shaken CdSe/octadecane/oleic acid/ethanol emulsion; (c) solution b after centrifugation; (d) solution after the removal of cloudy ethanol from c; (e) ethanol only; (f) residual CdSe after several centrifugation steps; (g) final completed isolated CdSe quantum dot nanoparticles from octadecane; and (h) different sizes of quantum dots. (B) UV–visible spectra of CdSe quantum dot nanoparticles with different particle sizes (from a to e, particle size increases).

100% ethanol. The prepared mixture was then gently shaken to obtain an emulsion (Figure 1Ab). This was then spun at 3000 rpm in a Maraton microA centrifuge for 5 minutes following which CdSe QDs suspension was collected from the top of the mixture of the ethanol (with some octadecane), while octadecane remained in the bottom of the tube (Figure 1Ac). This cloudy looking ethanol–octadecane layer (Figure 1Ac,d) was removed carefully with a syringe. The washing process was repeated several times until shaking no longer resulted in a suspension and the ethanol was no longer cloudy (Figure 1Ae). After several washings most of the octadecane is removed from the suspension (Figure 1Af). Finally, the ethanol was poured out and quantum dot nanoparticles of different sizes were isolated by the same procedure (Figure 1Ag). Absorption spectra of CdSe quantum dot nanoparticles in oleic acid and octadecane were performed with a Jasco V-550 UV-Vis Spectrophotometer. Wavelengths were chosen in the range 450–700 nm. PMMA cuvettes were used and disposed of after each experiment.

Characterization of Nanofibers. For morphology and diameter analyses of PVP/Ti (IV) isopropoxide and TiO_2 nanofibers, scanning electron microscopy (JEOL JSM-6360LV FESEM) at 15 kV was used. For SEM imaging, the samples were coated with gold to a thickness of approximately 100 Å to reduce charging. For nanofiber diameter distribution determination Image-J software was used to measure at least 50 nanofibers from each SEM image. OriginPro 8.1 software was used for statistical analyses of fiber diameter distributions and data chart preparations.

The crystal structures of TiO_2 nanofibers calcined at different temperatures were examined with wide angle X-ray diffraction and Raman Spectroscopy. A Philips XLF ATPS XRD 1000 (OMNI Instruments) customized with auto mount and a Cu Kα radiation source was used for XRD measurements. Diffraction patterns were collected from 20° to 80° at a rate of 5 deg/min. Raman spectra were measured at room temperature with a Horiba Jobin Yvon LabRam Aramis Microscope and with the laser line at 632 nm using a HeNe as an excitation source. Photoluminescence measurement was conducted using a Horiba Jobin Yvon LabRam/PL with He–Cd laser excitation source at 325 nm to observe crystal defects and to perform optical analyses of TiO_2 nanofibers calcined at different temperatures.

Bi-Functional Surface Modification and Incorporation of CdSe QDs to Electrospun TiO_2 Nanofibers. The surfaces of TiO_2 nanofibers are relatively inert, and they do not have functional groups to enable then to bond with CdSe quantum dots. Consequently, the surfaces of the calcined TiO_2 nanofiber mats were modified with a bi-functional chemical reagent, 3-mercaptoprionic acid (3-MPA), which contains both carboxylic (–COOH) and thiol (–SH) functional groups. A similar approach has been used by Gao and co-workers to link CdTe to a TiO_2 nanotube array.[2] A schematic illustration of the incorporation of CdSe nanoparticles to TiO_2 nanofibers via a one-step surface modification technique and the chemical mechanism of the process are shown in Figure 2.

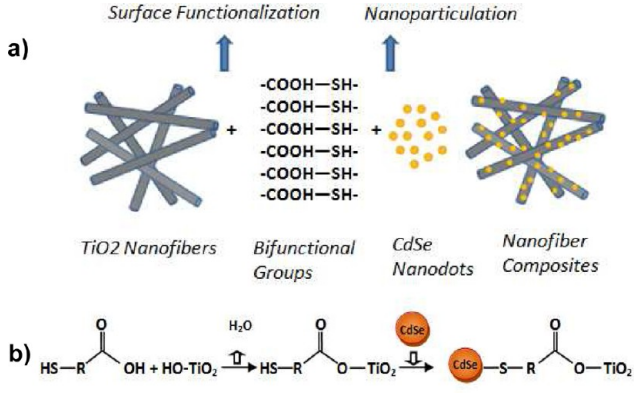

Figure 2. (a) Schematic representations of the 3-MPA surface functionalization of TiO_2 nanofibers and incorporation of CdSe quantum dots on them and (b) the chemical mechanism of the process.

First, TiO_2 nanofiber mats were immersed in 3-mercaptopropionic acid for 24 h. They were then rinsed three times with THF and allowed to dry in a fume hood. Since TiO_2 has a strong affinity for the carboxylate group of the linker molecules,[2] a bifunctional monolayer of 3-mercaptopropionic acid (3-MPA) was adsorbed on the surface of TiO_2 nanofibers. CdSe quantum dot nanoparticles could be bonded with the thiol groups of linker molecules.[30] To facilitate the incorporation of CdSe QD nanoparticles to electrospun TiO_2 nanofibers, CdSe nanoparticles were suspended in THF and sonicated for 10 minutes. The chemically modified TiO_2 nanofiber mats of equal

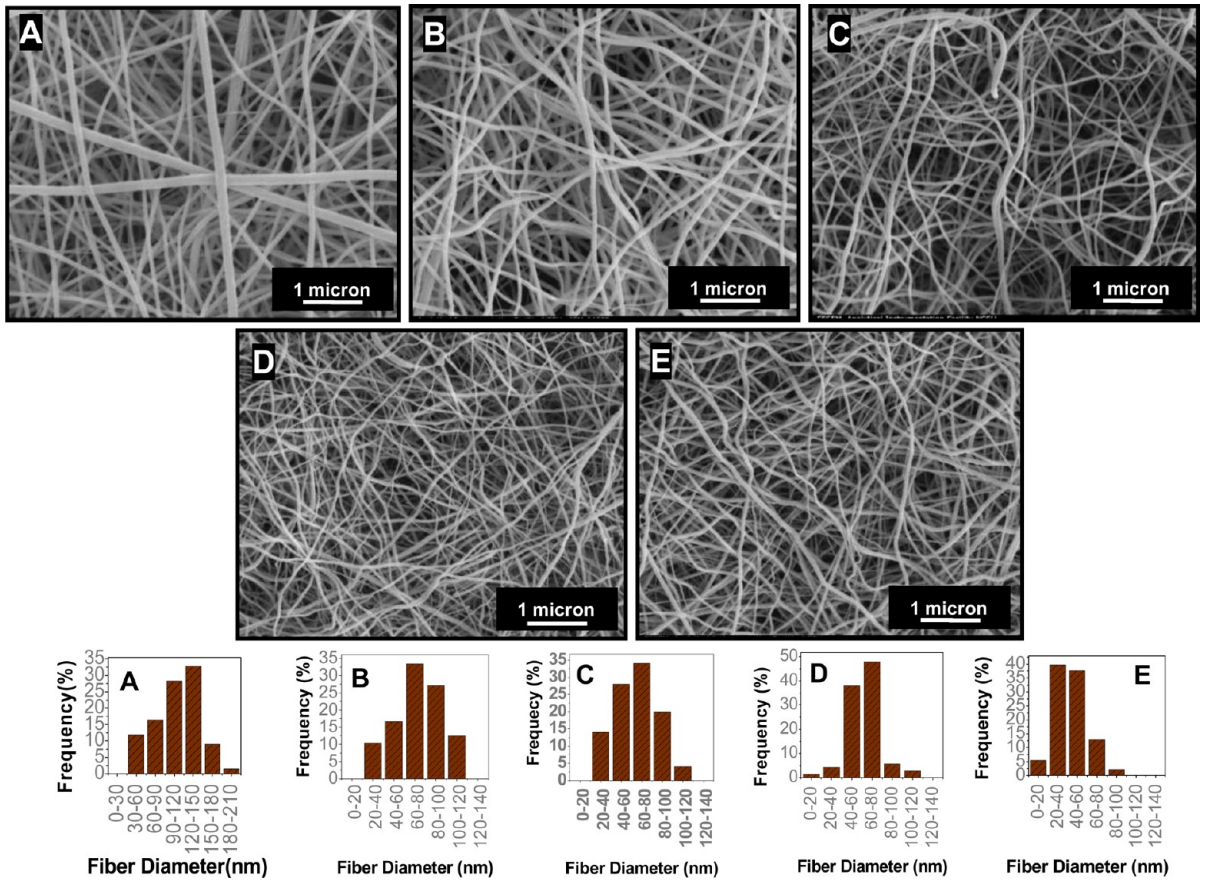

Figure 3. Scanning electron micrographs (low magnifications) and nanofiber diameter distributions of (A) Ti (IV) isopropoxide/PVP composite nanofibers and TiO_2 nanofibers calcined at (B) 400, (C) 500, (D) 650, and (E) 800 °C. Letters in the fiber distribution correspond to the image letters.

weight were then soaked in the THF suspension of CdSe QD nanoparticles for 24 h at ambient condition. The TiO_2 nanofibers which had been immersed in CdSe suspension turned from white to yellow to red in color depending on CdSe particle size, providing indirect evidence of CdSe adsorption into the nanofiber surface. The CdSe/TiO_2 composite nanofiber mats were rinsed again with THF three times to remove un-linked CdSe QD nanoparticles from the fibers.

Characterization of QD Templated TiO_2 Nanofibers. Attenuated total reflection Fourier transform infrared spectra (ATR-FTIR) was performed using a Thermo Fisher Scientific Nexus 470 model to determine the formation of the bonds between the quantum dots and nanofibers in the wave number range of 3500−700 cm^{-1} at room temperature. At least 124 scans were collected to minimize the noise. Chemical elemental composition analyses of CdSe/TiO_2 composite nanofibers were carried out with Energy Dispersive X-ray spectroscopy (EDS) installed on a Hitachi S-3200 Scanning Electron Microscope. All chemical species used in the CdSe/TiO_2 composite nanofibers were detectable by EDS spectra. In order to determine CdSe QD adsorption on TiO_2 nanofibers, the samples were examined with Hitachi HF2000 transmission electron microscopy. First, CdSe/TiO_2 composite nanofibers were crushed, put in a glass vial with some ethanol and sonicated for 10 minutes. Next, an amount of the prepared mixture was dropped on a carbon coated copper TEM grid. The sample on the TEM grid was dried overnight in room conditions to remove the ethanol residue from the sample before imaging. Photo-excited electron injections from CdSe QDs to TiO_2 NFs, as well as crystal defects, were evaluated with photoluminescence spectroscopy at the same laser excitation source and wavelength as that used with TiO_2 nanofibers. In addition, nanofibers of the same average diameter and mass were used for samples with and without CdSe.

3. RESULTS AND DISCUSSION

Morphology of Ti (IV) Isopropoxide/PVP and TiO_2 Nanofibers. TiO_2 nanofibers were generated after the calcination of electrospun Ti(IV) isopropoxide/PVP nanofibers. Low and high resolution SEM images of these nanofibers before and after calcination at different temperatures are shown in Figures 3 and 4, respectively. The average fiber diameter decreased dramatically upon calcination, and the diameter reduction reached approximately 100% when the fibers were calcined at 800 °C (Figure 3A−E). The statistically calculated average nanofiber diameter of Ti (IV) isopropoxide/PVP composite nanofiber before calcination was about 109 nm with a standard deviation of ±35. The calculated average diameters of the TiO_2 nanofibers calcined at 400, 500, 650, and 800 °C were 77, 65, 62, and 43 nm, respectively, with standard deviations of ±33, 23, 15, and 17. Such reduction in diameter may be the result of the removal of the polymer carrier from the fibers and conversion of the ceramic precursor to TiO_2. (TGA analysis showing fiber weight loss with heating is shown for a representative sample in Supporting Information Figure 2). Interestingly, fiber diameter distribution tended to narrow with calcination at higher temperatures. This can be seen in both the calculated standard deviation results and in the distribution diagram in Figure 3(A−E).

High resolution SEM images in Figure 4 reveal the surfaces of electrospun composite Ti (IV) isopropoxide/PVP composite nanofibers before calcination to be smooth (Figure 4A); however, surface smoothness decreased with the removal of

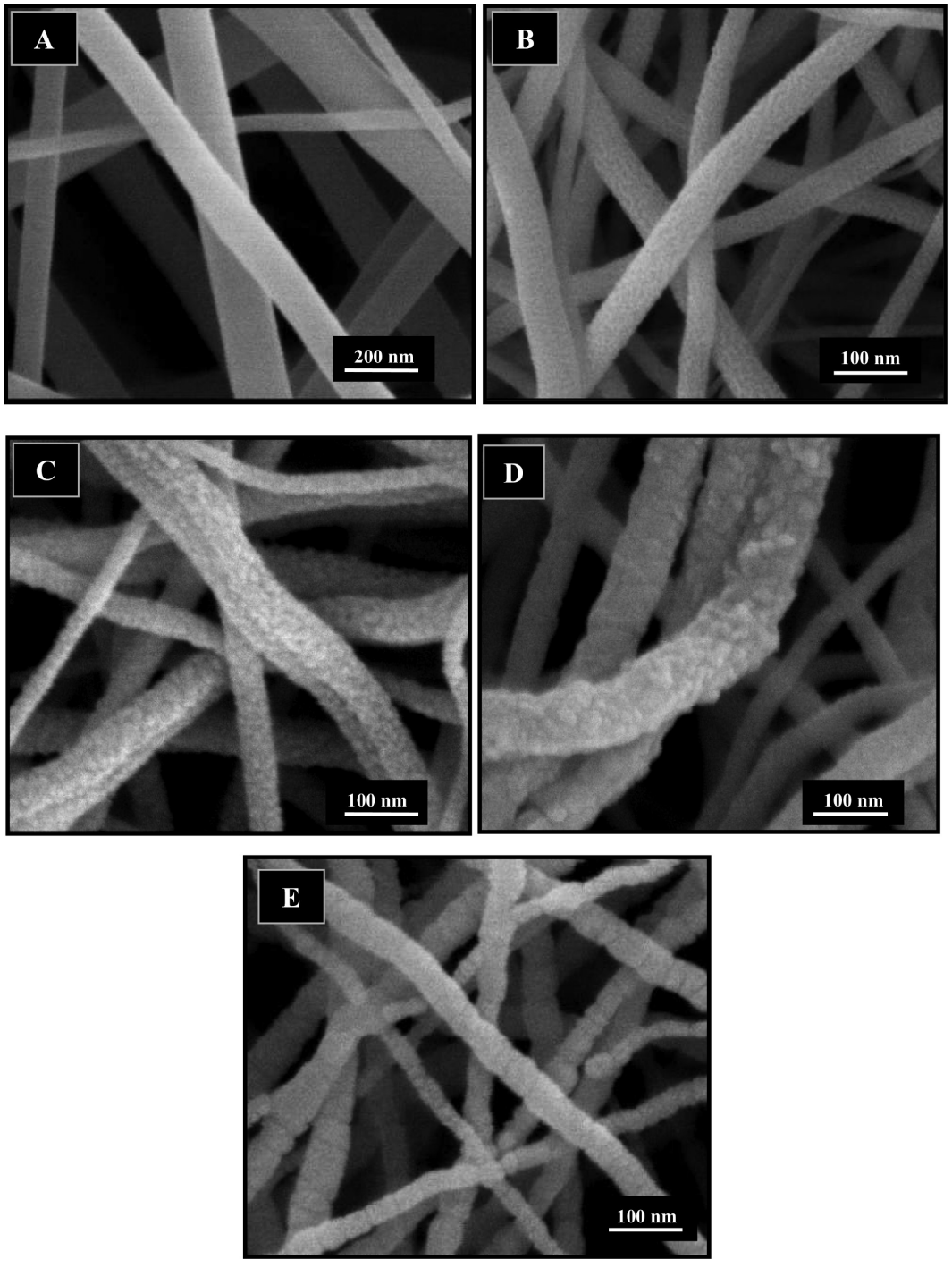

Figure 4. Scanning electron micrographs (high magnifications) of (a) Ti(IV) isopropoxide/PVP composite nanofibers and TiO_2 nanofibers calcined at (b) 400, (c) 500, (d) 650, and (e) 800 °C.

polymer and conversion of the ceramic precursor into ceramic nanofibers. The changes in surface structural features observed with different calcination temperatures (Figures 4B–E) may be attributed to a difference in crystal formation and transformations (anatase and rutile) of TiO_2 nanofibers, as discussed in subsequent sections and Supporting Information (Figure 3)

Crystal Structure of TiO_2 Nanofibers. X-ray diffraction analyses and Raman spectroscopic measurements were undertaken to verify changes in crystal structure with calcination and correlate with observed microscopy. XRD showed no crystalline peak on the sample before calcination since the sample was still amorphous (Supporting Information Figure 4); however, peaks began to appear at different 2θ degree intervals upon calcination.

As seen from Figure 5, electrospun TiO_2 nanofibers calcined at 400 and 500 °C have only anatase crystal structure and forms peaks at 2θ = 25.5° and 27.4° which correspond to the (101) and (002) crystal planes.[3] Samples calcined at 650°C show both anatase peaks at 2θ = 25.5°, 27.4°, 38.5°, 47.8°, 62.5° representing the indices of (101), (002), (112), (200), and (204), and rutile peaks at 2θ=27.7°, 36.1°, 41.2°, 43.9°, 54.4° corresponding to (110), (101), (111), (210), and (211) crystal

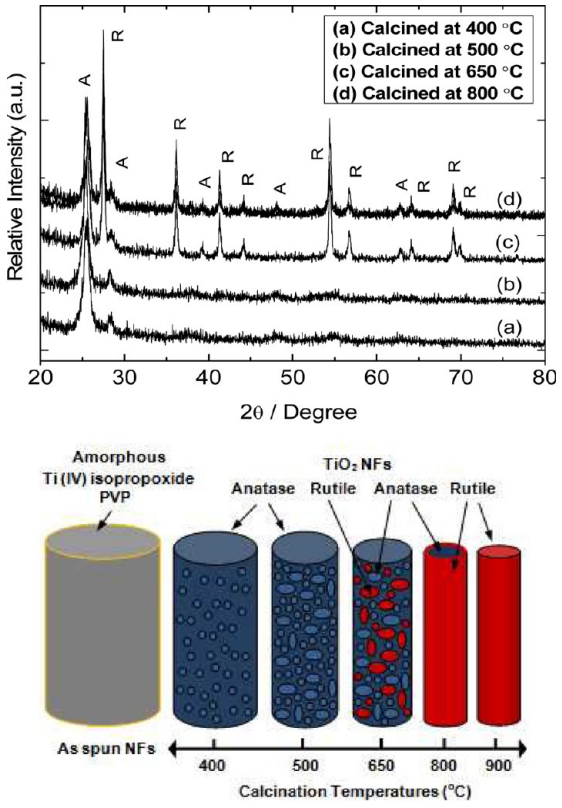

Figure 5. X-ray diffraction patterns of TiO_2 nanofibers calcined at (a) 400, (b) 500, (c) 650, and (d) 800 °C (top). Schematic illustration of phase transformation of TiO_2 nanofibers at different calcination temperatures (bottom).

planes of TiO_2. The spectral peaks of 56.5°, 63.9°, 68.5°, and 69.1° at 650 and 800 °C calcined samples are also the result of the rutile phase of TiO_2 crystals.[25,26,31−33]

The changes in crystal structure are also shown schematically in Figure 5 (bottom). When calcination temperature of the as-spun nanofibers are increased, small TiO_2 anatase crystals form. The quantity and sizes of the anatase crystals increase with increase in temperature from 400 to 500 °C. Rutile nuclei are formed on and at the interfaces among the anatase crystals, and the nanofiber samples undergo phase transformation from the anatase to the rutile in the temperature range between 550 and 680 °C.[3,7] At temperatures above 800 °C, most of the anatase crystals are transformed into the rutile phase and the fiber surfaces are smoother.

The schematic description of Figure 5 (bottom) seems to be consistent with the SEM images obtained after calcining at different temperatures (Figure 4). TiO_2 nanofiber samples calcined at 400 and 500 °C are in anatase form and the samples at 500 °C have larger anatase crystals, as can be seen from the fiber surfaces in Figure 5(B) and Figure 5(C). Upon further increase in the calcination temperature to 650 °C, the anatase crystal structures on the surface of nanofibers became larger (shown in Figure 5D) and rutile crystal phase started to form in bulk. Kumar et al.[34] mentions that bond breakage during the phase transformation causes the particle size to grow due to higher atomic motilities. At a higher calcination temperature of 800 °C, the anatase phase on the surface of TiO_2 nanofibers is transformed into the rutile phase and some small anatase crystals remain on the surface and in the bulk (Figure 5E). As also seen from the SEM image of the 800 °C calcined sample, the rutile phase of the surface of TiO_2 nanofibers can be seen as a smooth sausage-like form.

Evidence of the changes in crystal structure with calcination temperature was further obtained using Raman spectroscopy. The Raman spectra examined for nanofiber mat samples calcined at 400, 500, 650, and 800 °C are shown in Figure 6.

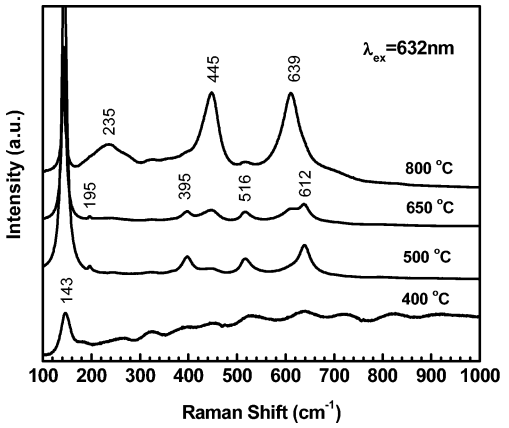

Figure 6. Raman Spectra of TiO_2 nanofibers calcined at 400, 500, 650, and 800 °C.

The samples calcined at 400 and 500 °C display major anatase Raman bands at 144, 196, 395, 516, and 639 cm^{-1}, which correspond to the six Raman-active modes of the anatase phase with the symmetries of E_g, E_g, B_{1g}, A_{1g}, and E_g, respectively.[1] At a higher calcination temperature of 650 °C, weak rutile crystal peaks are observed at the characteristic Raman bands at 143, 235, 445, and 612 cm^{-1}.[3] At a calcination temperature of 800 °C, the intensities of the peaks representing the anatase phase in the fibers decreases (395 and 639 cm^{-1}), and the intensities of rutile peaks at 445 and 612 cm^{-1} become stronger as a result of phase transformation from anatase to rutile in the structure. It should be noted that anatase to rutile volume fraction can be estimated from both the results of XRD and Raman spectra. XRD results give crystal information of both the surface and bulk, whereas Raman spectra (UV Raman, λ_{ex} = 325 nm) gives information on only surface crystalline states of TiO_2. Because photoluminescence is also a surface phenomenon, we use the Raman results to qualitatively discuss the relative amount of anatase to rutile volume fraction in this work.

Photoluminescence Analyses of TiO_2 Nanofibers. The optical properties and crystal defects of the semiconductive TiO_2 nanofibers calcined at 400, 500, 650, and 800 °C were investigated by photoluminescence (PL) spectroscopy. It has been well established that defects such as oxygen vacancies and/or titanium interstitials exist in both the anatase and rutile crystalline phases of TiO_2.[35,36] The photoluminescence properties of the materials closely correspond to the surface features of the material that could be changed remarkably by the annealing processes.[37] The location of the luminescence bands are correlated to the crystalline phases of TiO_2 nanofibers, with defect related crystalline microstructural change affecting the photoluminescence property of TiO_2.[10,38] Figure 7 shows the photoluminescence spectra of TiO_2 nanofiber samples calcined at 400, 500, 650, and 800 °C. We observe no band-edge transition for the rutile phase (at 3.0 eV corresponding approximately to 400 nm) or the anatase phase (at 3.2 eV corresponding approximately to 378 nm). Rather, we observe low energy peaks which may be attributed to material defects

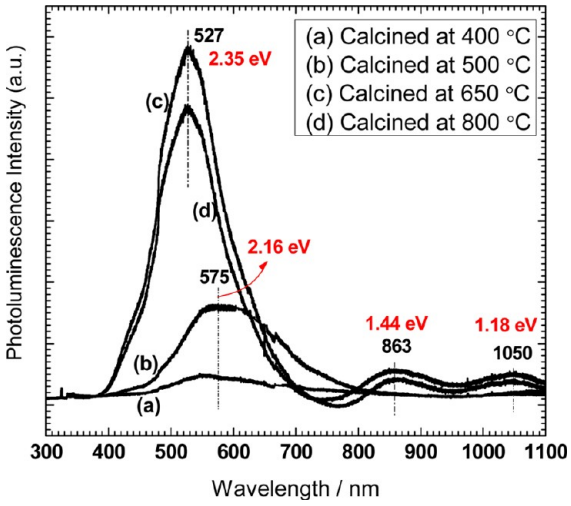

Figure 7. Photoluminescence spectra of TiO_2 nanofibers calcined at (a) 400, (b) 500, (c) 650, and (d) 800 °C.

such as oxygen vacancies. Such defect-mediated photoluminescence is consistent with studies reported on TiO_2 nanoparticles.[10]

The samples calcined at 400 and 500 °C are pure anatase TiO_2 nanofiber samples as observed from XRD data in Figure 5. The PL spectra of the sample calcined at 400 °C display a weak visible luminescence band located at 575 nm which increases in intensity in the sample calcined at 500 °C. When the calcination temperature was increased to 650 °C (appearance of rutile phase, Figure 5 bottom), two weak near-infrared luminescence bands appear (centered at 863 nm and 1050 nm) and the band in the visible region become stronger and shifts from 575 to 527 nm. When the calcination temperature was increased to 800 °C (more rutile phase formed, Figure 5 bottom) the intensity of the 527 nm band is weakened and the intensities of 863 and 1050 nm bands become stronger.

It has been reported that the peaks centered in the near-infrared bands are related to the intrinsic defects in the rutile phase of TiO_2 nanofibers, while the peaks located in the visible luminescence band are correlated to oxygen vacancies in the anatase phase of TiO_2 nanofibers, and that the intensity of the emission peaks increase with the defect levels.[1] So, we can surmise that the oxygen vacancy defect increases in TiO_2 nanofibers when the calcination temperature increases from 400 to 500 °C and to 650 °C, and decreases when the samples are calcined at 800 °C because phase transformation changes the defect type from oxygen vacancy to intrinsic defect. Hence, the near infrared intensity of the sample calcined at 800 °C is stronger than that of the sample calcined at 650 °C (Figure 7).

UV−Visible Spectra of As Synthesized CdSe Quantum Dots. UV-visible spectra were carried out to evaluate absorption properties of the synthesized CdSe quantum dots. Quantum dots are semiconductive nanoparticles and exhibit a dramatic property change through changes in their shapes and sizes. As seen from the inset in Figure 1B, the color of the CdSe quantum dots in octadecane and oleic acid solvent changes from yellow to red depending on the particle size, as particle size increases from a to e. In the inset, the first sample (yellow) was extracted from the reaction media after adding all the chemical components in the reaction mixture, and other samples were extracted sequentially from the reaction media in 10 second intervals. With a longer reaction time, CdSe particle size increases and the solution color turns from yellow to red. The observable peak maxima were detected at UV-Visible absorption spectra in the visible region with the range of wavelength values between 500 nm and 600 nm. The maximum peak shifts were from violet to green, and the absorbance increased due to the increase in particle size (Figure 1B). A similar trend was reported by Nordell et al.[13] Comparison of the absorption of the TiO_2 nanofiber mat with that of a representative sample of quantum dot (QD sample c in Figure 1B) is demonstrated in the Supporting Information section (Supporting Information Figure 6).

Surface Functionalized TiO_2 NFs with CdSe QDs. To ensure that surface templating of TiO_2 nanofibers with QDs were indeed achieved using a bifunctional ligand (Figure 2), three different experimental approaches were conducted. First, the adsorption and binding of monolayer of 3-MPA to TiO_2 nanofibers and bond formation between the 3-MPA and CdSe quantum dot nanoparticles were characterized by ATR-FTIR technique, and the spectra were recorded in the spectral range from 700 to 3500 cm^{-1} (Figure 8). Because PVP degrades and

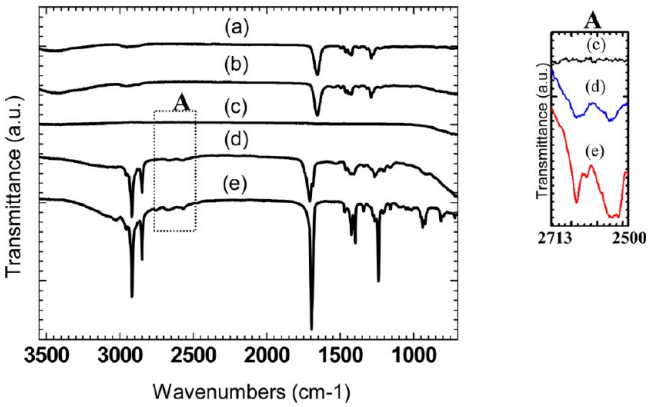

Figure 8. ATR-FTIR spectra of (a) PVP nanofibers, (b)PVP/Ti(IV)isopropoxide composite nanofibers, (c) TiO_2 nanofibers calcined at 500°C, (d) CdSe(small particle)/TiO_2 composite nanofibers, and (e) CdSe (big particle)/TiO_2 composite nanofibers.

is removed from the nanofibers during the calcinations process, all the peaks coming from PVP disappeared in the TiO_2 nanofiber sample after calcination, as can be seen in Figure 8c. The weak absorption at 2569.5 cm^{-1} of the CdSe/TiO_2 sample can be ascribed to the −SH stretching in the case of the bond formation between CdSe QDs and the 3-MPA monolayer on TiO_2 NFs (Figure 8d and e including enlarged inset A). The intensity of this peak becomes stronger with the use of larger particles. Also, in Figure 8d, since the small particles links to the TiO_2 nanofiber sample, a weak band of 1645 cm^{-1} is observed as a result of the formation of interchain disulfide.[39] This leads to less particle incorporation to TiO_2 nanofibers. Over all, the intensities of the absorption peaks became stronger when large particles are used, as seen in Figures 8d and Figure 9e. The Cd−Se band stretching is located at ∼722 cm^{-1}.[40] Except ∼722 cm^{-1}, the band stretching below 1500 cm^{-1} comes from the 3-MPA monolayer on TiO_2 nanofibers. The peaks at 2852 and 2925 cm^{-1} can be attributed to the $\nu_{as}(CH_2)$ and $\nu_s(CH_2)$ vibrational modes of the long alkyl chain of oleic acid ligands between CdSe and TiO_2 nanofibers.[41]

After the CdSe quantum dot nanoparticle-linked TiO_2 nanofibers were washed with THF three times, the samples

dx.doi.org/10.1021/am300524a | ACS Appl. Mater. Interfaces 2012, 4, 3837−3845

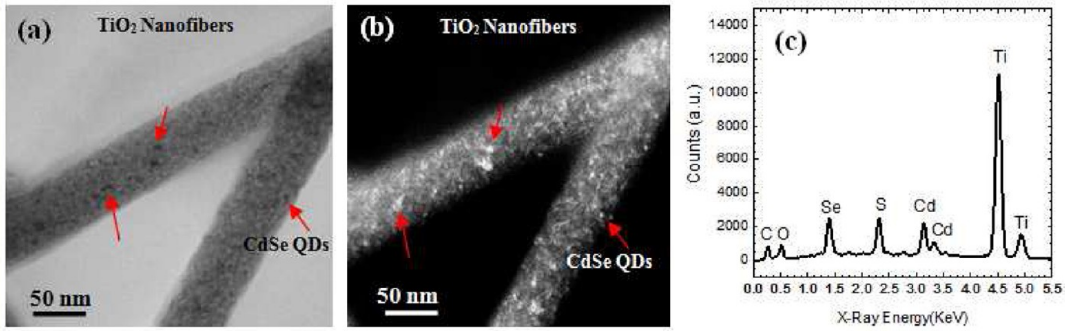

Figure 9. Bright field (a) and dark field (b) TEM images, and (c) energy dispersive X-ray spectra (EDS) of CdSe/TiO_2 composite nanofibers.

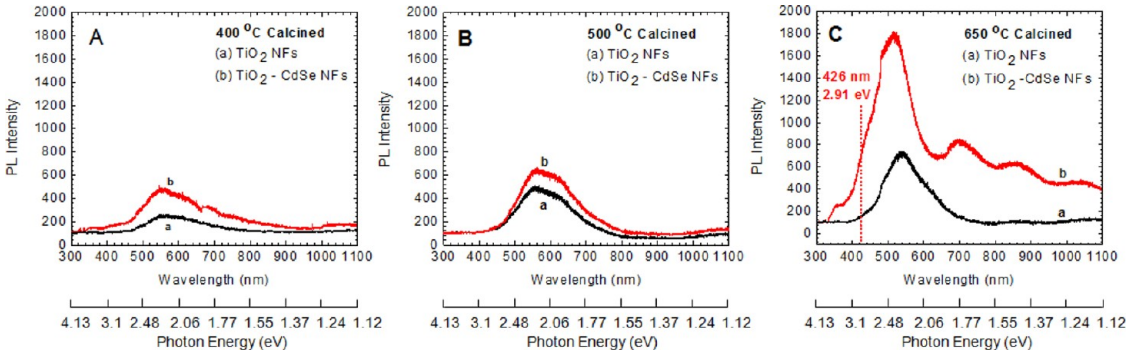

Figure 10. Photoluminescence spectra of TiO_2 and TiO_2−CdSe nanofibers calcined at (A) 400, (B) 500, and (C) 650 °C.

were placed in a fumed hood for several days for drying. Bright and dark field transmission electron microscopy images of TiO_2/CdSe composite nanofibers are shown in Figure 9 for further visual verification of the presence of QDs on the nanofibers. The locations of CdSe quantum dots on the TiO_2 nanofibers are pointed to by arrows in the TEM image. In the bright field TEM image (Figure 9a), CdSe quantum dots on the nanofibers correspond to the dark spots, while in dark field TEM image (Figure 9b), they correspond to the bright spots.

Finally, the dried CdSe/TiO_2 composite nanofiber samples were analyzed with the EDS for chemical elemental analyses. As seen from the EDS spectra in Figure 9c, each chemical element in the composite CdSe/TiO_2 nanofiber structure displays its own corresponding peak at a specific detected X-ray energy. The sample shows peaks at ∼4.5 and ∼4.88 KeV for titanium (Ti), ∼3.11 and ∼3.28 KeV for cadmium (Cd), ∼2.29 KeV for sulfur (S) (which comes from the bi-functional linker), ∼1.38 KeV for selenium (Se), ∼0.46 KeV for oxygen (O), and ∼0.23 KeV for carbon (C) (which also comes from the bi-functional linker molecule). All of the peaks on the EDS spectra are in agreement with the work reported by Zhang et al.[42]

Photoluminescence Analyses of TiO_2−CdSe Quantum Dot Nanofibers. Photoluminescence emission measurements of TiO_2 and CdSe-TiO_2 nanofibers with the TiO_2 nanofibers calcined at three different temperatures (400, 500, and 650 °C) are shown in Figure 10. When CdSe QDs are incorporated to TiO_2, an increase in the total luminescence emission intensity is observed for all CdSe-TiO_2 composite nanofibers (Figure 10 A-C). Because of the different conduction band (CB) edge positions of CdSe and TiO_2 (shown in Supporting Information Figure 5), photo-excited electron injection possibly occurs from the high conduction band CdSe QDs to the lower conduction band TiO_2 nanofibers. As a result, when CdSe quantum dots are embedded or linked to TiO_2, photoluminescence emission increases for CdSe-TiO_2 composite nanofiber structures compared to TiO_2 only nanofibers. In all cases, we find that the defect-mediated photoluminescence is enhanced by the presence of quantum dots. In addition, the sample calcined at 650 °C now shows additional signals above 3.2 eV corresponding to band edge emission. Abazovic and co-workers found a strong peak at 2.91 eV corresponding to band-edge emission for TiO_2 nanoparticles.[10] We observe a strong enhancement of such signal in our sample with the addition of QDs.

The PL intensity change for a sample calcined at 500°C (Figure 10B) is lower than that of a sample calcined at 400 °C (Figure 10A) because the presence of more anatase crystals in the 500 °C-annealed sample yield better CdSe−TiO_2 interactions, and the excited electron trapped in the oxygen vacancies of the crystals are easily transferred to TiO_2. The adsorption of CdSe quantum dots by rutile-type TiO_2 crystals are higher than the anatase-type TiO_2 up to a certain degree of rutile content; so the most significant photoluminescence enhancement is at 650 °C (Figure 10C), corresponding to TiO_2 sample with the highest degree of crystallinity, in the presence of both anatase and rutile phases.[43−45]

4. CONCLUSIONS

In this study, electrospun TiO_2 nanofibers was generated via the sol−gel electrospinning technique and phase transformation of the TiO_2 crystals after subjecting the nanofibers to different calcination temperatures was examined. The incorporation of as-synthesized CdSe quantum dot nanoparticles onto TiO_2 nanofibers via the bi-functional (3-MPA) linker-assisted adsorption (LA) method was also performed. Photo-excited electron injection from CdSe QDs to TiO_2 NFs (calcined at 400, 500, 650, and 800 °C) was evaluated via photoluminescence spectroscopy. Nanofiber diameter de-

creased significantly after calcination and crystal phase transformation from anatase to rutile was observed at higher calcination temperatures. The 400 and 500 °C calcined TiO_2 nanofiber samples demonstrated only the anatase phase in the fiber structure while the 650 and 800 °C calcined samples have both anatase and rutile phases in the fiber structures. Formation of a CdSe/TiO_2 composite structure was shown via FTIR and EDS spectra, and TEM imaging. Photo-excited electron injection from CdSe QDs to TiO_2 NFs (calcined at 400, 500, and 650 °C) were conducted via photoluminescence spectroscopy. PL results reveal that crystal phases in TiO_2 nanofibers play an important role on photo-excited electron injection from quantum dots to TiO_2 nanofibers. Photoluminescence emission intensities increase dramatically with the addition of CdSe QDs in all TiO_2 nanofiber samples, and the presence of a small amount of rutile in bulk anatase crystals leads to more electron injection from CdSe QDs to TiO_2 nanofibers.

■ ASSOCIATED CONTENT

Ⓢ Supporting Information

Schematic of sol−gel electrospinning and calcination, TGA analysis during heating of nanofibers, crystal form changes with heat treatment, XRD spectra of before and after calcined nanofibers, and electronic band-edge position of bulk CdSe with anatase and rutile TiO_2. This material is available free of charge via the Internet at http://pubs.acs.org.

■ AUTHOR INFORMATION

Corresponding Author

*E-mail: khan@eos.ncsu.edu. Phone: 919 515-4519.

Present Address

[§]DuPont Central Research and Development, 200 Powder Mill Road, Wilmington, DE 19880-0304, United States

Notes

The authors declare no competing financial interest.

■ ACKNOWLEDGMENTS

The authors acknowledge funding support from the Nonwovens Cooperative Research Center, NCRC at North Carolina State University and the Ministry of National Education of the Republic of Turkey. Y.A. thanks Mr. Chuck Mooney, Mr. Roberto Garcia, and Dr. Dale Bachelor of the Analytical Instrumentation Facility, NCSU, and Dr. Mark D. Walters of the Shared Materials Instrumentation Facility at Duke University for their assistance in sample characterization.

■ REFERENCES

(1) Shi, J.; Chen, J.; Feng, Z.; Chen, T.; Lian, Y.; Wang, X.; Li, C. *J. Phys. Chem. C* **2007**, *111*, 693−699.
(2) Gao, X. F.; Li, H. B.; Sun, W. T.; Chen, Q.; Tang, F. Q.; Peng, L. M. *J. Phys. Chem. C* **2009**, *113*, 7531−7535.
(3) Zhang, J.; Li, M.; Feng, Z.; Chen, J.; Li, C. *J. Phys. Chem. B* **2006**, *110*, 927−935.
(4) Zhang, X.; Xu, S.; Han, G. *Mater. Lett.* **2009**, *63*, 1761−1763.
(5) Takahashi, K.; Yui, H. *J. Phys. Chem. C* **2009**, *113*, 20322−20327.
(6) Park, N. G.; Lagemaat, J. V. D.; Frank, A. J. *J. Phys. Chem. B* **2000**, *104*, 8989−8994.
(7) Zhang, J.; Xu, Q.; Feng, Z.; Li, M.; Li, C. *Angew. Chem., Int. Ed.* **2008**, *47*, 1766−1769.
(8) Tanaka, K.; Capule, F. V. M; Hisanaga, T. *Chem. Phys. Lett.* **1991**, *187*, 73−76.
(9) Kim, J. Y.; Jung, H. S.; Noh, J. H.; Kim, J. R; Hong, K. S. *J. Electroceram.* **2006**, *16*, 447−451.
(10) Abazovic, N.D.; Comor, M.I.; Dramicanin, M.D.; Jovanovic, D.J.; Ahrenkiel, S.P.; Nedeljkovic, J.M. *J. Phys. Chem. B.* **2006**, *110*, 25366−25370.
(11) Lee, J. C.; Sung, Y. M. *Appl. Phys. Lett.* **2007**, *91*, 113104.
(12) Trindade, T.; Brien, P.O. *Adv. Mater.* **1996**, *8*, 161−163.
(13) Nordell, K. J.; Boatman, E. M.; Lisensky, G. C. *J. Chem. Educ.* **2005**, *82*, 1697−1699.
(14) Wijayantha, K. G. V.; Laurence, L. M.; Peter, M.; Otley, L. C. *Sol. Energy Mater. Sol. Cells* **2004**, *83*, 363−369.
(15) Lee, Y. L.; Huang, B. M.; Chien, H. T. *Chem. Mater.* **2008**, *20*, 6903−6905.
(16) Kamat, P. V. *J. Phys. Chem. C* **2008**, *112*, 18737−18753.
(17) Sero, I. M.; Gimenez, S.; Santiago, F. F.; Gomez, R.; Shen, Q.; Toyoda, T.; Bisquert, J. *Acc. Chem. Res.* **2009**, *42*, 1848−1857.
(18) Wang, W.; Huang, H.; Li, Z.; Zhang, H.; Wang, Y.; Zheng, W.; Wang, C. *J. Am. Ceram. Soc.* **2008**, *91*, 3817−3819.
(19) Mukherjee, K.; Teng, T. H.; Jose, R.; Ramakrishna, S. *Appl. Phys. Lett.* **2009**, *95*, 012101.
(20) Zhang, W.; Zhu, R.; Liu, X.; Liu, B.; Ramakrishna, S. *Appl. Phys. Lett.* **2009**, *95*, 043304.
(21) Guo, C. S.; Xu, J. A.; He, Y.; Zhang, Y. A.; Wang, Y. Q. *Appl. Surf. Sci.* **2011**, *257*, 3798−3803.
(22) Christy, P. D.; Melikechi, N.; Jothi, N. S. N.; Suganthi, A. R. B.; Sagayaraj, P. *J. Nanopart. Res.* **2010**, *12*, 2875−2882.
(23) Wu, T.; Tao, J.; Deng, J.; Tang, Y. X.; Zhu, H.; Gao, P. *Acta Phys. Chim. Sin.* **2010**, *26*, 3087−3094.
(24) Kemell, M.; Pore, V.; Ritala, M.; Leskela, M.; Linden, M. *J. Am. Chem. Soc.* **2005**, *127*, 14178−14179.
(25) Kumar, A.; Jose, K.; Fujihara, K.; Wang, J.; Ramakrishna, S. *Chem. Mater.* **2007**, *19*, 6536−6542.
(26) Chuangchote, S.; Sagawa, T.; Yoshikawa, S. *Appl. Phys. Lett.* **2008**, *93*, 033310.
(27) Kang, S. H.; Kumar, C. K.; Lee, Z.; Kim, K. H.; Huh, C.; Kim, E. T. *Appl. Phys. Lett.* **2008**, *93*, 191116.
(28) Yu, H. Z.; Peng, J. B. *Org. Electron.* **2008**, *9*, 1022−1025.
(29) Munro, A. M.; Ginger, D. S. *Nano Lett.* **2008**, *8*, 2585−2590.
(30) Mann, J. R.; Watson, M. D. *Langmuir* **2007**, *23*, 10924−10928.
(31) Okimura, K.; Furumi, T. *Jap. Soc. Appl. Phys.* **2004**, *43*, 655−658.
(32) Tan, T. F.; Wang, S. R.; Bian, S. G.; Li, X. G. *Adv. Mater. Res.* **2009**, *79*, 385−388.
(33) Wongkaew, A.; Jansome, W.; Khemchan, S.; Sawaengmit, N.; Mitpapan, S. *Energy Research Journal* **2010**, *1*, 73−77.
(34) Kumar, K. N. P. *Scripta Metall. Mater.* **1995**, *32*, 873−877.
(35) Henderson, M. A. *Surf, Sci.* **1999**, *419*, 174−187.
(36) Valentin, C.D.; Pacchioni, G.; Selloni, A. *J. Phys. Chem. C.* **2009**, *113*, 20543−20552.
(37) Zacharias, M.; Fauchet, P. M. *Appl. Phys. Lett.* **1997**, *71*, 380.
(38) Smith, D. L.; Mailhiot, C. *Rev. Mod. Phys.* **1990**, *62*, 173−234.
(39) Tetenbaum, J.; Miller, L. M. *Biochemicstry* **2001**, *4*, 12215−12219.
(40) Hamizi, N. A.; Johan, M. R. *Mater. Chem. Phys.* **2010**, *124*, 395−398.
(41) Liu, L.; Hensel, J.; Fitzmorris, R. C.; Li, Y.; Zhang, J. Z. *J. Phys. Chem. Lett.* **2010**, *1*, 155−160.
(42) Zhang, H.; Quan, X.; Chen, S.; Yu, H.; Ma, N. *Chem. Mater.* **2009**, *21*, 3090−3095.
(43) Zhao, L.; Han, M.; Lian, J. *Thin Solid Films* **2008**, *516*, 3394−3398.
(44) Toyoda, T.; Tsuboya, I.; Shen, Q. *Mater. Sci. Eng., C* **2005**, *25*, 853−857.
(45) Luke, T. L.; Wolcott, A.; Xu, L.; Chen, S.; Wen, Z.; Li, J.; Rosa, E.D.L.; Zhang, J. Z. *J. Phys. Chem. C* **2008**, *112*, 1282−1292.